IOPscience iopscience.iop.org

Home Search Collections Journals About Contact us My IOPscience

An optical study of alkali-metal vapour zones produced by thermal evaporation in helium gas

This article has been downloaded from IOPscience. Please scroll down to see the full text article.

1994 J. Phys.: Condens. Matter 6 7303

(http://iopscience.iop.org/0953-8984/6/36/013)

View the table of contents for this issue, or go to the journal homepage for more

Download details:
IP Address: 171.66.16.151
The article was downloaded on 12/05/2010 at 20:28

Please note that terms and conditions apply.

J. Phys.: Condens. Matter 6 (1994) 7303–7316. Printed in the UK

An optical study of alkali-metal vapour zones produced by thermal evaporation in helium gas

Shōsuke Mochizuki† and Raphael Ruppin‡

† Department of Physics, College of Humanities and Sciences, Nihon University, 3-25-40 Sakurajosui, Setagaya-ku, Tokyo 156, Japan

‡ Department of Physics and Applied Mathematics, Soreq NRC, Yavne 70600, Israel

Received 29 April 1994

Abstract. We have measured the time-resolved and space-resolved optical spectra of sodium and potassium vapour zones produced by thermal evaporation in helium gas. The structure of the spectra and their time dependence indicate that atoms evaporate first and later dimers and clusters grow by coalesence in the vapour zone. Information on the size trends of the clusters and microcrystals is derived from the time evolution of the surface-plasmon extinction band. For clusters the position of the band is interpreted in terms of the spill-out effect, while for microcrystals it is calculated from the Mie theory with a size-dependent correction to the dielectric constant.

1. Introduction

The optical properties of alkali-metal clusters have attracted much attention recently, because they provide information about the evolution of physical characteristics from the atom to the bulk solid. For this purpose, it is best to produce a free-cluster stream that contains size-selected clusters and to measure the optical properties as a function of size. Many photoabsorption measurements of this type have been performed on alkali metals, limited mainly to small clusters. This type of experiment has recently been reviewed by de Heer (1993). In the large-particle limit, optical spectra of alkali-metal microcrystals, with typical sizes of the order of 20 nm, have been obtained by the gas-evaporation method, in which the metal is evaporated under a low-pressure noble gas (Mann and Broida 1973). We have recently shown that by setting appropriate conditions for the gas evaporation and by measuring time-resolved and space-resolved (at various positions above the evaporation source) transmission spectra, the whole range of species sizes can be observed (Mochizuki 1991, 1992, Mochizuki and Ruppin 1993, Mochizuki 1993). The process of dimer, cluster and microcrystal growth can be monitored by observing the evolution of the optical spectra with time. In the present paper we report the details of our experiments on sodium and potassium and identify the various features appearing in the time-resolved and space-resolved optical spectra.

2. Experimental details

Experiments were carried out using the apparatus described previously (Mochizuki 1991, 1992, Mochizuki and Ruppin 1993, Mochizuki 1993). A Pyrex glass crucible (inner diameter

0953-8984/94/367303+14$19.50 © 1994 IOP Publishing Ltd

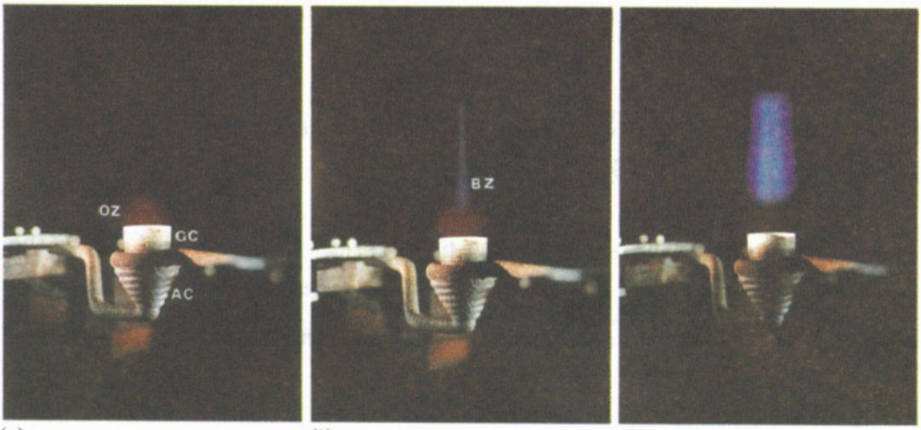

Figure 1. A typical view of the gas evaporation of sodium: OZ, orange-fluorescence zone; BZ, blue zone; GC, glass crucible; AC, alumina crucible heater.

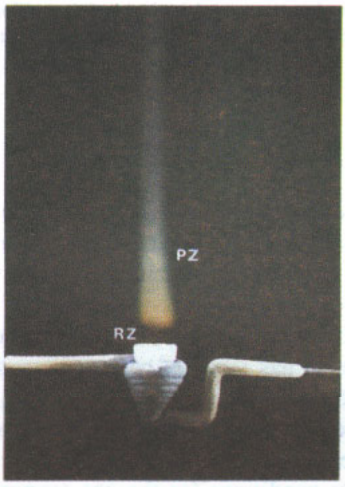

Figure 6. A typical view of the gas evaporation of potassium: RZ, red zone; PZ, pinkish orange zone.

of 6 mm) containing nominally pure alkali metal was heated indirectly in an alumina crucible on which a tungsten-wire heater was wound. The temperature of the glass crucible was gradually increased by applying a constant voltage. Prior to the optical measurements the temperatures of the crucible and of representative positions in the vapour zone were measured with a thermocouple under the same condition of gas evaporation at which the optical measurements would be made. Optical spectra of selected positions in the vapour zone were recorded in a transmission configuration as a function of time elapsed from the beginning of the evaporation. Continuum light from a 150 W xenon lamp was directed at the whole zone above the crucible through an optical window without using a lens. After passing the vapour zone, only the light through a selected position was collected by a lens, spectrally analysed and recorded by an optical multichannel analyser system. The transmission at a given height is the intensity ratio of the transmitted radiation during the gas evaporation process to that of the transmitted radiation through the same position before the

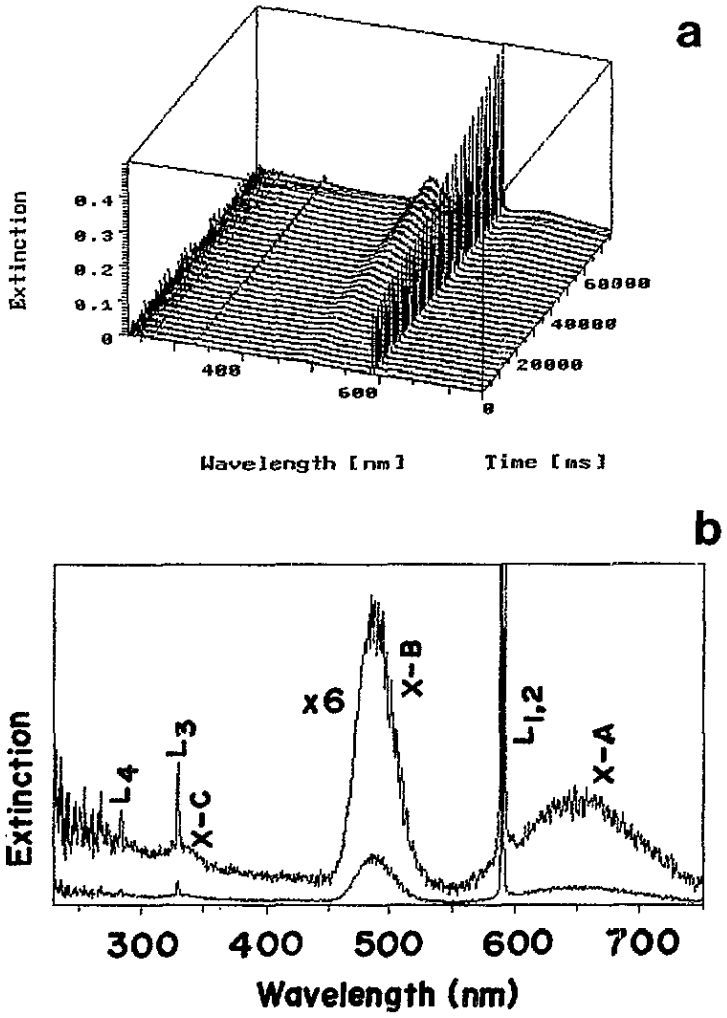

Figure 2. (a) The time evolution of the extinction spectrum of the sodium orange zone at a height of 3 mm above the crucible edge. (b) The 32nd spectrum of the time-resolved spectrum (a).

beginning of the evaporation. Since the transmission spectra T_t obtained contain the effects of both scattering and absorption, the results are expressed as extinction spectra $-\log T_t$.

3. Results

3.1. Sodium

By setting appropriate evaporation conditions we were able to produce several separate zones at different heights above the evaporation source, one containing atoms and dimers and another containing clusters and microcrystals. Figure 1 shows a typical view of the gas evaporation of sodium in confined helium gas at 140 Torr. This figure was obtained under illumination of white light (xenon lamp), with the evaporation carried out

at crucible temperatures higher than 573 K. Figures 1(a), (b) and (c) correspond to the initial, intermediate and final stages of the gas evaporation. As seen in figure 1(a), at the beginning stage, an orange emission zone (OZ) appears just above glass crucible (GC). The orange emission is due to fluorescence from sodium atoms, Na, the so-called D lines of sodium. With progressing evaporation, an elongated blue scattering zone (BZ) appears above the orange zone. Although not discernible in this figure, a pale green emission inside the orange emission zone is observable by the naked eye. The green emission is due to fluorescence from sodium dimers, Na_2. As mentioned later, the blue scattering is due to resonance scattering by surface plasmons of sodium clusters and microcrystals, $Na_n (n > 2)$. On further progressing gas evaporation, the blue scattering zone grows to produce a thick multi-layer cone. All optical measurements were carried out before the appearance of such a multi-layer cone structure.

Figure 2(a) shows the time evolution of the extinction spectrum of the orange zone at a height of 3 mm above the crucible edge. The time-resolved display consists of 32 spectra. The 32nd spectrum is shown in figure 2(b). At the initial stage of gas evaporation, the spectrum is dominated by sharp atomic absorption lines at about 589 nm ($L_{1,2}$), about 330 nm (L_3) and about 285 nm (L_4). These wavelengths are close to those reported in the literature (White 1934). This indicates that initially the majority of evaporated species are sodium atoms, with the lines arising from the electronic transitions from S state to P states. With progressing gas evaporation, these absorption lines become stronger, which indicates that the concentration of Na vapour increases. At later times the three weak bands appear and grow between 310 and 360 nm (C band), between 460 and 520 nm (B band) and between 560 and 750 nm (A band). These bands correspond to the X–C, X–B and X–A electronic vibrational transitions of sodium dimer, Na_2, respectively (Rosen 1970).

Figure 3(a) shows the time evolution of the extinction spectrum of the blue zone at 23 mm above the crucible. Three spectra, the 10th, 20th and 32nd, are shown in figure 3(b). Again, the spectrum is that of atomic sodium at early stages. With progressing gas evaporation, a weak broad band appears at about 478 nm, together with a shoulder band at about 370 nm. At later times the broad band grows and the peak wavelength shifts to about 450 nm. This band is due to the collective plasma mode resonance. Since the average cluster size increases with time, the results shown in figure 3 indicate that the frequency of the plasma resonance increases with increasing cluster size. This is due to the corresponding decrease of the spillout effect (Parks and McDonald 1989, Selby *et al* 1991, Bréchignac *et al* 1992a, b), as will be discussed in detail in the next section. The observed very broad band width may be due to cluster aspherical distortion and cluster size distribution.

The data of figure 3(a) yield information about the process of cluster growth during the evaporation. This can be seen more clearly by plotting the time dependence of the peak wavelength of the plasma resonance (figure 4(a)) and the peak extinctions due to atomic sodium, Na, and due to sodium clusters Na_n (figure 4(b)). In figure 4(b) each curve is normalized to its maximum value. It is found that the extinction due to Na increases with time, reaching a maximum at about 30–40 s, and then decreases slightly. Extinction due to Na_n begins only after about 9 s and then increases with time, with the rate of increase becoming higher after the inflection point at about 25 s. This indicates that the formation of clusters from the Na vapour begins after the concentration of the latter has reached some threshold value. All the spectra discussed so far were obtained in a confined helium environment at 140 Torr. Under these conditions microcrystals (i.e., very large clusters) are not easily formed. In order to investigate this size region as well, we have performed gas evaporation in a helium gas stream of pressure lower than 1 Torr, with a flow rate of 1 l min^{-1}. The time evolution of the extinction spectra of the vapour zone at a height of

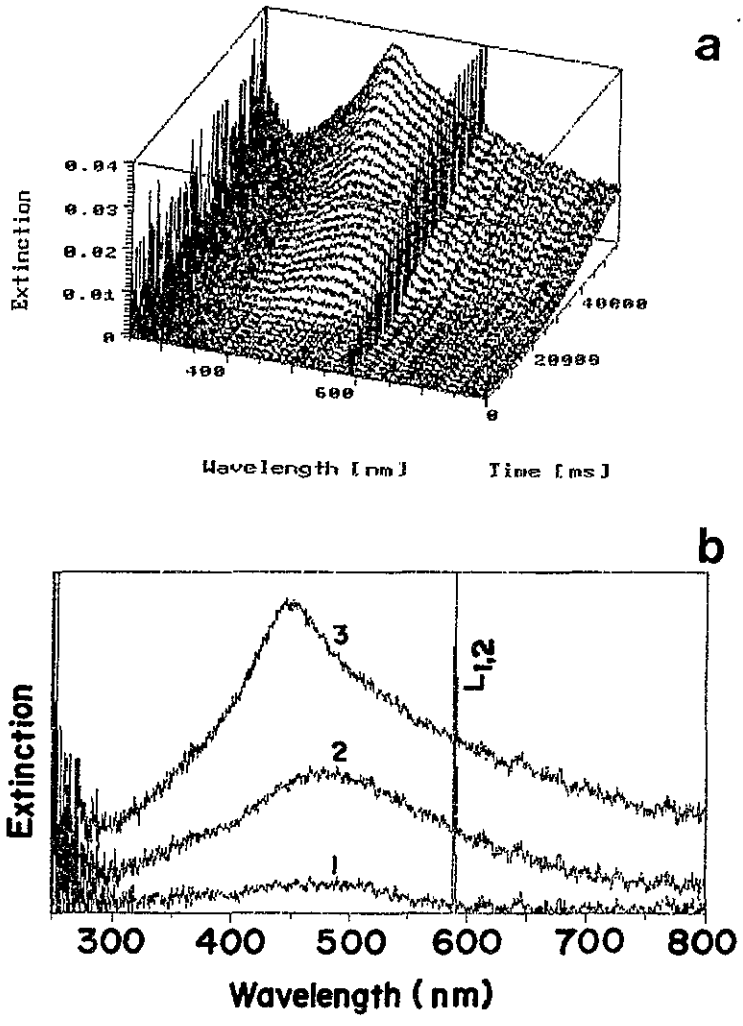

Figure 3. (a) The time evolution of the extinction spectrum of the sodium blue zone at a height of 23 mm above the crucible edge. (b) Various spectra of the time-resolved spectrum (a). The spectra 1,2 and 3 correspond to the 10th, 20th and 32nd spectra, respectively.

6 mm above the crucible is shown in figure 5. At first only atomic lines appear, but later the spectrum is dominated by the surface-plasmon band, which forms at about 375 nm. With progressing gas evaporation this band shifts towards the long-wavelength side while its bandwidth decreases. At later stages, when steady-state evaporation is approached, the bandwidth begins to increase and the peak frequency reaches the value of about 405 nm. At these stages a broad tail also appears at the long-wavelength side.

3.2. Potassium

Figure 6 shows a typical view of the gas evaporation of potassium at 573 K in confined helium gas of 180 torr under the illumination of a xenon lamp. In this figure there appears a dark red zone (RZ), ranging from the glass crucible to a height of about 5 mm, and above it a conical pinkish orange fluorescence zone (PZ). This zone structure of the potassium

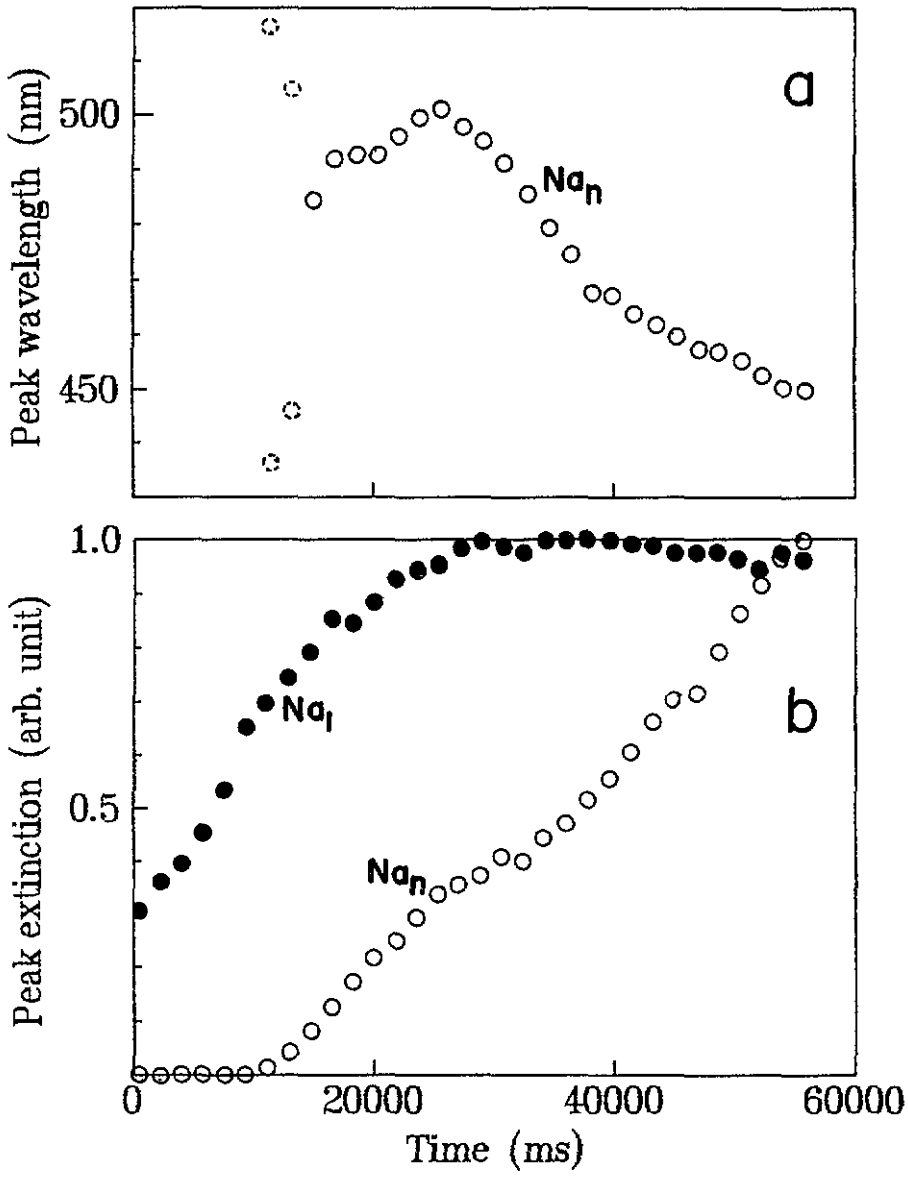

Figure 4. (a) The time dependence of the peak wavelength of the Na_n band. (b) The time dependence of the extinction of the $Na(Na_1)$ and Na_n bands.

vapour is very sensitive to the shape of the evaporation source, which consists of the glass crucible and the alumina crucible heater, the pressure and the flow rate of the gas and the evaporation temperature, as was also observed for silver (Mochizuki 1993). For example, when the crucible temperature was raised to 700 K, the pinkish orange fluorescent zone grew into a large cone, which was composed of several subcone shells.

We have measured the extinction spectra at various positions in these zones. Spectra obtained at the steady state of gas evaporation at heights of 3, 20, 35 and 40 mm above the crucible edge are shown by figure 7(a)–(d), respectively. During the evaporation, the

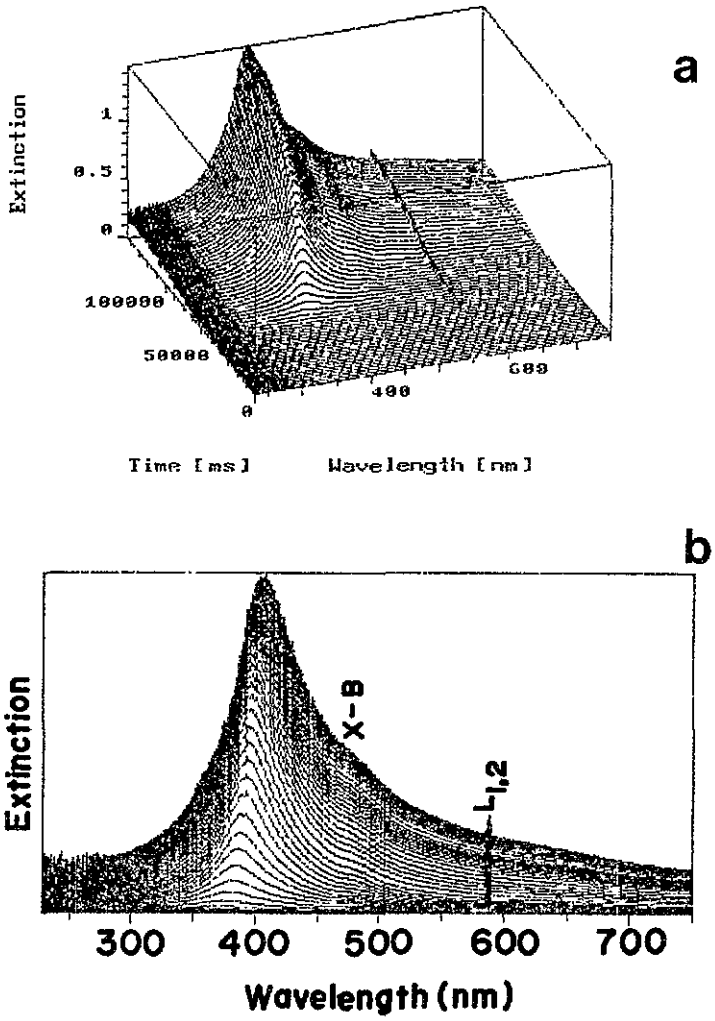

Figure 5. The time evolution of the extinction spectrum of the sodium vapour zone at a height of 6 mm above the crucible edge in a low-pressure helium gas stream.

temperature of the glass crucible rose to 573 K. As shown in figure 7(a), at the dark red zone near the crucible, three sharp doublet lines, $L_{1,2}$, $L_{3,4}$ and $L_{5,6}$, appear at about 767 nm, about 404 nm and about 345 nm, respectively. These wavelengths are close to those of the known S–P electronic transitions in atomic potassium (White 1934): 766.5 and 769.9 nm for 4S–4P transitions, 404.4 and 404.7 nm for 4S–5P transitions and 344.6 and 344.7 nm for 4S–6P transitions. Also, a broad band with fine structure is seen between 620 and 690 nm, which is assigned to the electronic-vibrational transition X–B of K_2, be referring to a spectroscopic table (Rosen 1970). Figure 8 shows the time dependence of the ratio of the extinction due to K_2 to that due to K, which was deduced from the time-resolved spectra measured at the height of 3 mm from the crucible edge. Since the extinction due to K and K_2 is proportional to the number of each species, this curve is proportional to the number ratio of K_2 and K. At the beginning the number of dimers is very small, and only at about 30 s does it begin to grow. From about 50 s the K_2/K number ratio begins to increase at a higher rate. Thus,

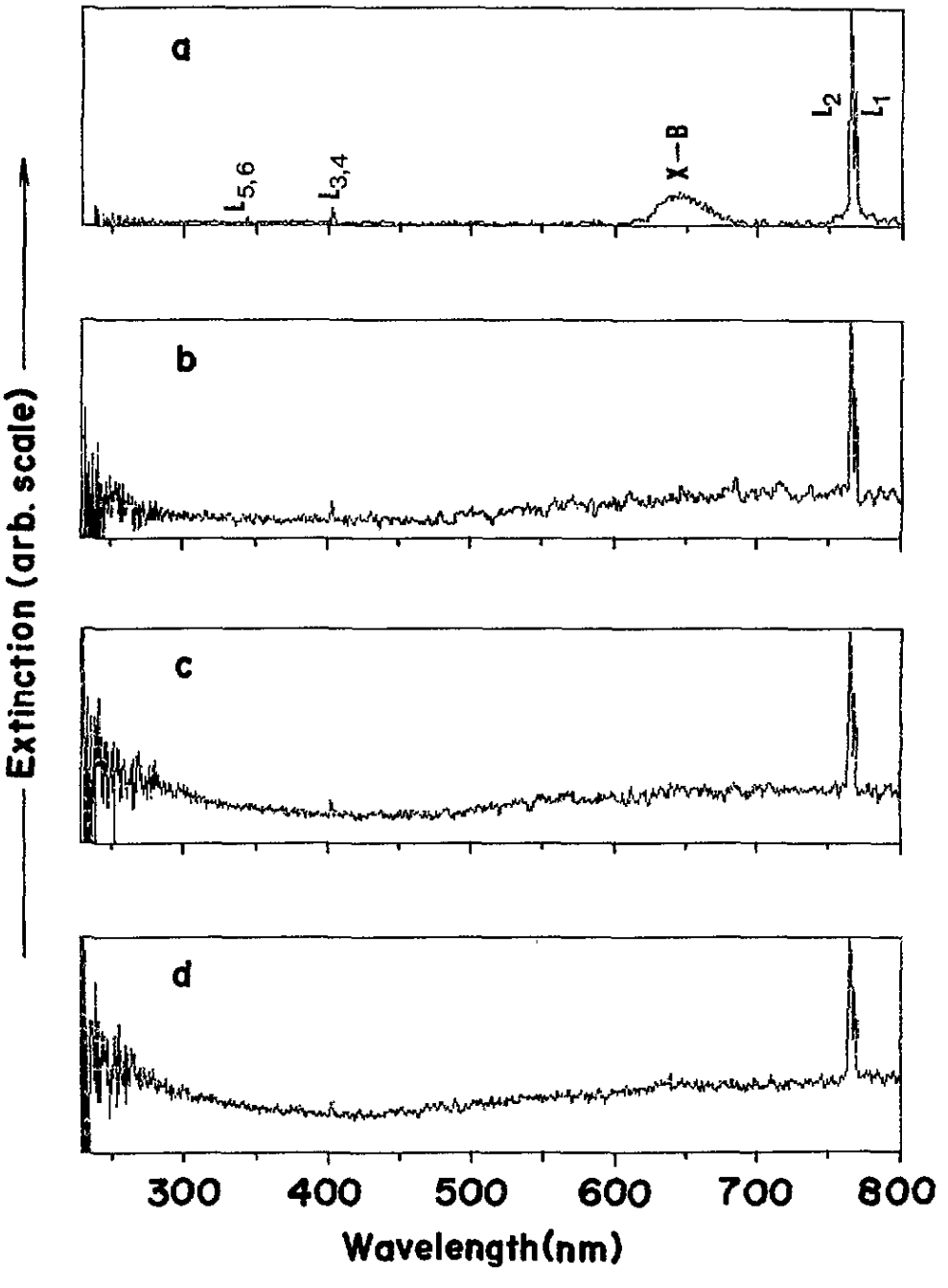

Figure 7. Space-resolved extinction spectra of the potassium vapour zone. Evaporation was carried out in confined helium gas at 140 Torr. The heights from the crucible edge are as follows: (a) 3 mm; (b) 20 mm; (c) 35 mm; (d) 40 mm.

after some concentration of evaporated potassium atoms is attained, dimers are produced by coalescence of atoms. The X–C, X–D, X–E, X–F and X–G transitions are buried in the faint

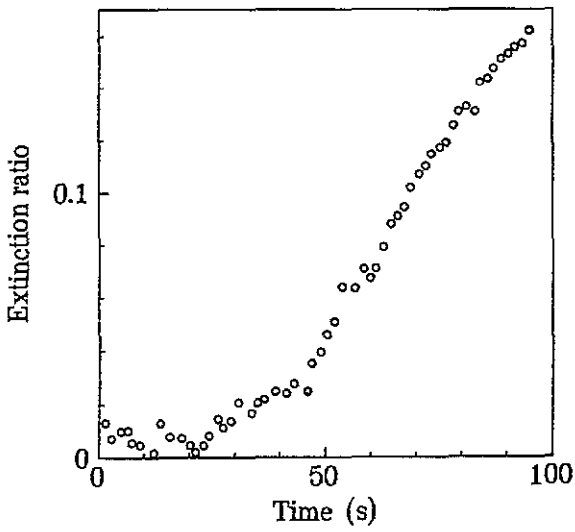

Figure 8. The time dependence of the ratio of the extinction due to K_2 to that due to K at a height of 3 mm above the crucible edge.

broad extinction band between 300 and 450 nm. With increasing height into the pinkish orange fluorescence zone, the absorption lines due to K survive, but those due to K_2 become weak, while broad extinction bands begin to grow both at shorter- and longer-wavelength regions than 400 nm, as shown in figures 7(b), (c) and (d). Since the long-wavelength band cannot be assigned to any electronic transition due to K_2, it is probably due to potassium clusters K_n ($n > 2$). However, a clear collective mode resonance does not appear. In order to obtain microcrystals and to observe the collective plasma resonance, we again resort to the flowing-gas configuration. The time-resolved extinction spectra obtained at a height of 6 mm, in a stream of helium gas of pressure 2 Torr and flow rate 0.5 l min^{-1} is shown in figure 9. At the early stages a very broad band due to K_2 and sharp lines due to K appear at about 640 and about 767 nm, respectively. With progressing gas evaporation, a broad band appears at 564 nm (spectrum 2). Later this broad band grows, decreases in width, and shifts to the shorter wavelength of 549 nm (spectrum 3). At still later times this band, which is due to the plasma resonance, moves back to longer wavelengths, up to 584 nm, and increases in width (spectra 4 and 5). In order to observe the microcrystal growth process in more detail, we have performed an evaporation at a higher pressure of 3 Torr, a higher flow rate of 2.5 l min^{-1}, and a slower heating rate. The 64 time-resolved spectra recorded in this experiment are shown in figure 10(a). The 34th, 45th, 50th, 54th, 58th and 64th spectra are shown in figure 10(b). At an early stage a broad band appears at about 559 nm. With increasing time this band gradually shifts to the long-wavelength side, while its width decreases at first and later increases again. This is the trend which the plasma resonance of microcrystals is expected to follow when their size increases, as will be demonstrated by the calculations presented in the next section.

4. Discussion

We could not determine directly the sizes and shapes of the clusters and microcrystals, because of their high reactivity with atmospheric moisture. However, for some of the observed spectra we can estimate the average particle size from the energy and shape of the plasma extinction band. We recall the main properties of the plasma band and its evolution

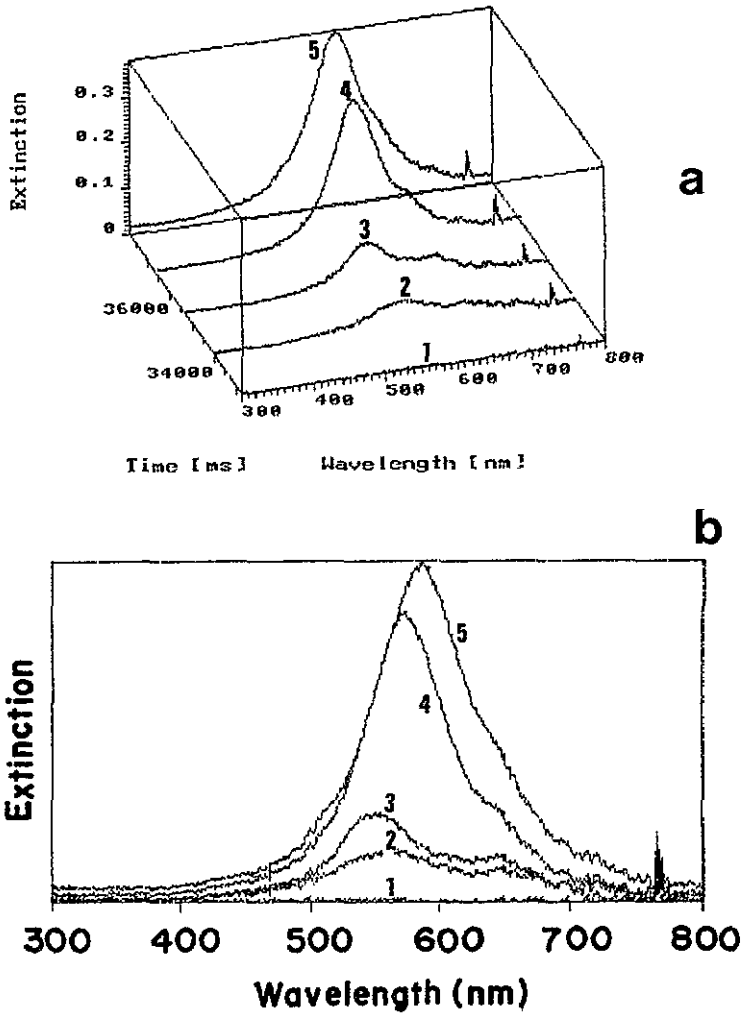

Figure 9. The time evolution of the extinction spectra of the potassium vapour zone in a low-pressure helium gas stream.

with increasing particle size. In the very-small-size region, i.e., for clusters containing from tens up to hundreds of atoms, the surface-plasmon absorption resonance is shifted considerably from the classical Mie value towards the low-frequency side. This arises from the spillout effect of the valence electrons, which are distributed over a radius slightly larger than the ionic core radius (Parks and McDonald 1989, Selby *et al* 1991, Bréchignac *et al* 1992a, b). This effectively reduces the electron density, and hence the plasma frequency, in small clusters. This red shift decreases with increasing cluster size. For small, open-shell clusters there may also occur a splitting of the plasmon peak into two or three peaks, due to the spherical or ellipsoidal shape of the clusters (Selby *et al* 1991). With increasing size, for radii larger than about 2 nm, the so-called microcrystal region is reached. The plasma resonance of a spheroidal microcrystal occurs at $\omega_p/\sqrt{3}$, where ω_p is the bulk plasma frequency. For small microcrystals the band is much wider than that calculated from the Mie theory using the bulk value of the dielectric constant. This happens when the microcrystal

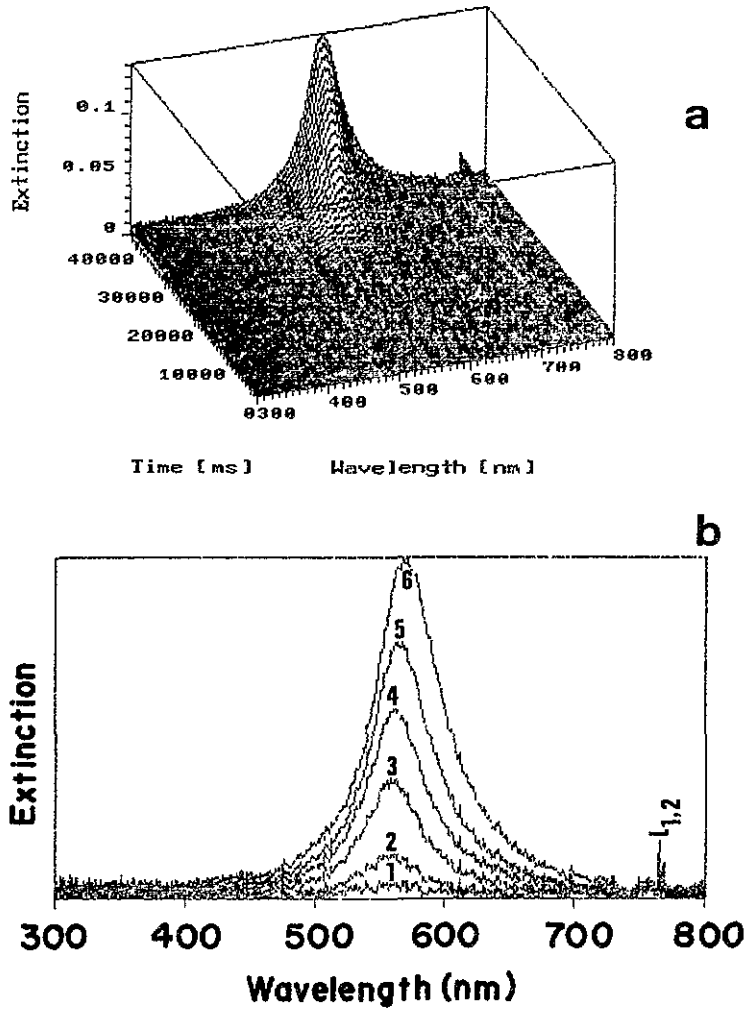

Figure 10. (a) The detailed time evolution of the extinction spectrum of potassium microcrystals in a low-pressure helium gas stream. (b) Several spectra of the time-resolved spectrum (a). The spectra 1, 2, 3, 4, 5 and 6 correspond to the 34th, 45th, 50th, 54th, 58th and 64th spectra, respectively.

size is comparable with the electron mean free path. The collisions of the conduction electrons with the particle surface become important as an additional collision process and thus the effective mean free path is smaller than in the bulk (Kreibig and Fragstein 1969). This leads to an increase of the imaginary part of the dielectric constant, and a corresponding broadening of the absorption band. With increasing microcrystal size this free-path effect decreases, and hence the plasma absorption band becomes narrower. When the microcrystal size increases beyond about 10 nm, the absorption bandwidth begins to increase again, this time due to the onset of radiative broadening. The radiative contribution also causes the centre of the band to shift towards the low-frequency side.

For sodium, in the spectra of figure 3 the contribution of clusters is clearly seen. The first few spectra are very broad (e.g., the 10th spectrum, curve 1 of figure 3(b)). This is probably due to both the multi-peak structure of non-spherical clusters and cluster-size

distribution. At later times, when the average cluster size increases, a clear plasma band is formed (spectra 2 and 3 of figure 3(b)). Figure 4(a) shows that from the 15th spectrum onwards the wavelength of the plasma peak decreases monotonically with time, i.e., with increasing cluster size. This is due to the decrease of the spill-out effect. By comparing with the data of Parks and McDonald (1989) for the dependence of the resonance frequency on cluster size, we estimate that the lowest wavelength observed (the 15th spectrum) is due to clusters containing an average number of about 12 atoms, while the shortest wavelength (the last spectrum) arises from clusters containing an average of about 26 atoms.

In figure 5 the absorption structure is dominated by the contribution of microcrystals. This will now be confirmed by a calculation based on the Mie theory, from which we will also obtain estimates of how the average microcrystal size increases with time. The values of the frequency-dependent dielectric constant, $\epsilon_1 + i\epsilon_2$, used in the calculations were taken from the experimental data of Smith (1969). These, however, refer to the bulk, and for small spheres have to be modified so as to account for the free-path effect discussed above. We introduce this size correction in the form suggested by Kreibig (1974), according to which the dielectric constant of a sphere of radius R is given by

$$\epsilon(R) = \epsilon_1 + i[\epsilon_2 + (\omega_p^2/\omega^3)(v_F/R)]. \tag{1}$$

Here ω_p is the plasma frequency and v_F is the Fermi velocity.

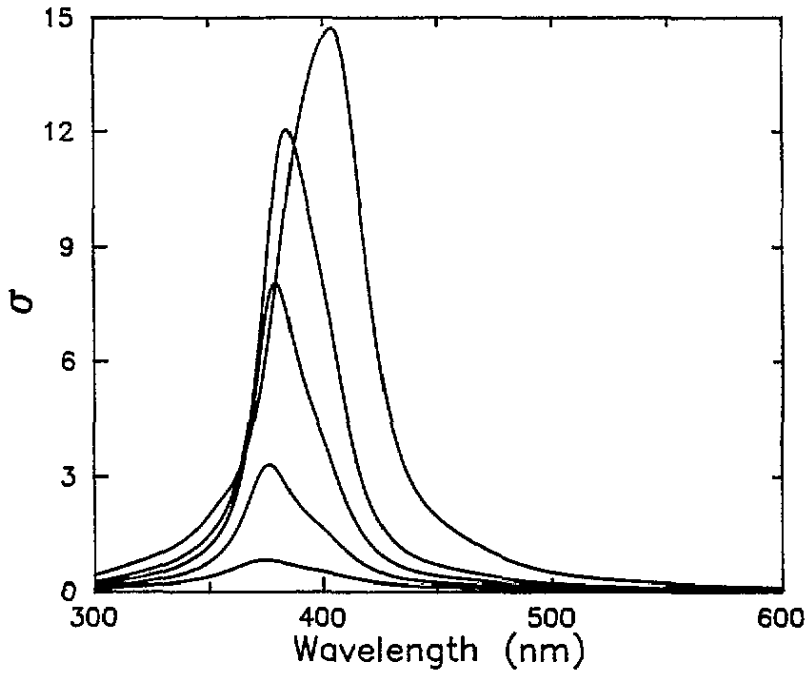

Figure 11. Calculated extinction spectra of sodium spheres for various radii: 2 nm (lowest curve), 5 nm, 10 nm, 15 nm, 24 nm.

Calculated extinction spectra of sodium spheres are shown in figure 11 for radii of 2, 5, 10, 15 and 24 nm. The calculated spectra exhibit the same gradual shift of the

peak to the long-wavelength side as observed experimentally in figure 5. Also, the width first decreases (due to the decrease of the free-path effect) and later increases again (due to radiative broadening), in agreement with the experimental results. One feature not reproduced by our calculations is the broad tail at the long-wavelength side. This is because the calculations were performed for a single sphere, whereas the tail arises from interactions between adjacent microcrystals, as has previously been demonstrated for silver microcrystals (Mochizuki and Ruppin 1993, Hayashi *et al* 1990).

For potassium confined in helium gas (figure 7) no clear plasma resonance was observed, which indicates that microcrystals were not formed. The very broad band at long wavelengths, seen in figures 7(b), (c) and (d), is probably due to small clusters. Also, this indicates that the smoky feature of the observed pinkish orange zone (figure 6) is due to the high density of such small clusters. In the flowing helium gas the collective mode resonance appears and its strength increases with time, i.e., with increasing average microcrystal size. The behaviour of the spectra shown in figure 10 can be understood by comparing with Mie-theory calculations. For these we have used the experimental data of Smith (1969) for the bulk dielectric constant, again employing the size-dependent correction (1). The results of the calculations for potassium spheres of radii 5, 10, 15, 20, 25 and 30 nm are shown in figure 12. As in the experimental spectra (figure 10), the width of the band first decreases and at later times begins to increase, while the peak shifts gradually to longer wavelengths. We thus obtain the estimate of 30 nm for the average radius of the largest microcrystals (spectrum 6 of figure 10).

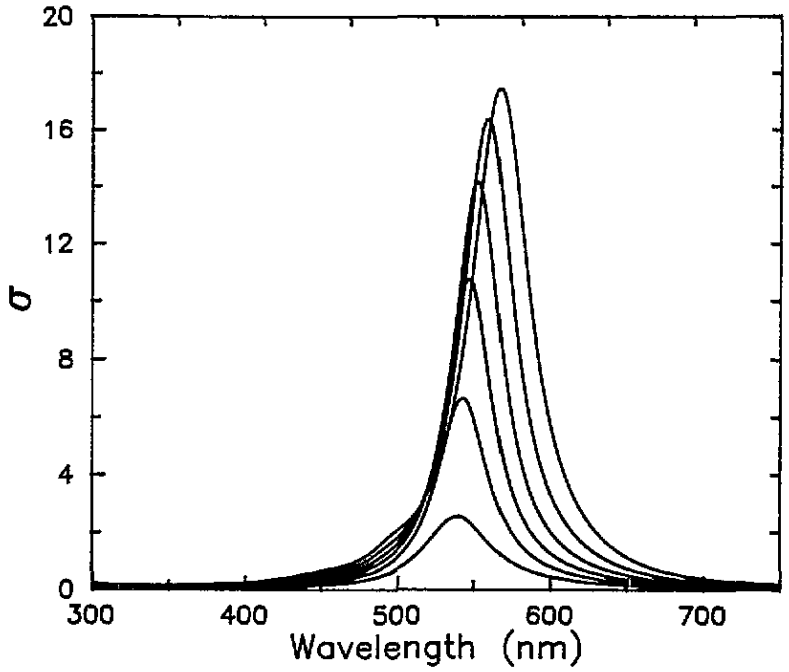

Figure 12. Calculated extinction spectra of potassium spheres for various radii: 5 nm (lowest curve), 10 nm, 15 nm, 25 nm, 30 nm.

In conclusion, we have produced vertically well separated vapour zones of sodium and of potassium by thermal evaporation in confined helium gas, and measured time-resolved

spectra of the various zones. The spectra indicate the occurrence of atoms, dimers and small clusters. We have also measured time-resolved spectra of the vapour zone produced by thermal evaporation in flowing helium gas. In this case a prominent plasma collective absorption band appeared, increasing in strength with time, thus indicating that microcrystals were being formed and growing with time.

The time evolution of the frequency of the collective mode resonance of clusters differs qualitatively from that of microcrystals. For clusters the peak shifts to higher frequencies with increasing size, due to the decrease of the spill-out effect. For microcrystals the peak shifts to lower frequencies, because with increasing size radiative effects begin to contribute.

Acknowledgments

This study was supported in part by a grant-in-aid for scientific research from the Ministry of Education (Japan). It was also supported in part by a grant-in-aid (1991, 1993) for overseas research from Nihon University.

References

Bréchignac C, Cahuzac Ph, Carlier F, de Frutos M and Leygnier J 1992a *Chem. Phys. Lett.* **189** 28
Bréchignac C, Cahuzac Ph, Kebaili N, Leygnier N and Sarfati A 1992b *Phys. Rev. Lett.* **68** 3916
de Heer W A 1993 *Rev. Mod. Phys.* **65** 611
Hayashi S, Koga R, Ohtuji M and Yamamoto K 1990 *Solid State Commun.* **76** 1067
Kreibig U 1974 *J. Phys. F: Met. Phys.* **4** 999
Kreibig U and Fragstein C V 1969 *Z. Phys.* **224** 307
Mann D M and Broida H P 1973 *J. Appl. Phys.* **44** 4950
Mochizuki S 1991 *Phys. Lett.* **155A** 510
—— 1992 *Phys. Lett.* **164A** 191
—— 1993 *Phys. Lett.* **176A** 382
Mochizuki S and Ruppin R 1993 *J. Phys.: Condens. Matter* **5** 135
Parks J H and McDonald S A 1989 *Phys. Rev. Lett.* **62** 2301
Rosen B 1970 *Spectroscopic Data Relative to Diatomic Molecules* (Oxford: Pergamon)
Selby K, Kresin K, Masui J, Vollmer M, de Heer W A, Scheidemann A and Knight W D 1991 *Phys. Rev.* B **43** 4565
Smith N V 1969 *Phys. Rev.* **183** 634
White H E 1934 *Introduction to Atomic Spectra* (New York: McGraw-Hill)